Radio Observations of Gyroresonance Emission from Coronal Magnetic Fields

S. M. White and M. R. Kundu
Dept. of Astronomy, University of Maryland
College Park, MD 20742 USA

Abstract. We review the basic characteristics of thermal gyroresonance (also known as cyclotron) emission from solar active regions, and show how radio observations combined with our understanding of the basic mechanism can reveal much of the magnetic and thermal structure of the corona over active regions.

1. Introduction

Since the realization in the early 1960s [Ginzburg & Zheleznyakov 1961; Kakinuma & Swarup 1962; Zheleznyakov 1962] that the strong radio emission observed from solar active regions was associated with gyroresonance opacity, radio observations have provided the only direct diagnostic of magnetic field strengths in the solar corona. It is a happy coincidence that the low harmonics of the range of magnetic field strengths found in the corona (up to 2500 G) correspond to the range of microwave frequencies ($1 - 20$ GHz) for which atmospheric transmission is not an issue and high spatial resolution radio observations are readily feasible. In view of the recent developments in the measurement of photospheric magnetic fields and techniques for their extrapolation into the solar corona (see recent reviews from the 1996 SCOSTEP Workshop on *Measurements and Analyses of the 3D Solar Magnetic Fields*, published in Solar Physics), it is timely to review the capabilities of radio measurements and to discuss their use in conjunction with optical magnetic data. In this review we discuss the ideas behind the use of radio observations to determine the physical conditions in the corona above active regions, and mention future developments which will lead to a major improvement in the results obtained from radio observations.

Both of the mechanisms responsible for opacity in the active region corona at radio wavelengths, gyroresonance emission and bremsstrahlung (free electrons deflected by ions and remaining unbound, hence also known as free–free emission), are sensitive to the magnetic field. Here we focus on the application of gyroresonance theory to the interpretation of the radio observations, since it is a more direct diagnostic of coronal magnetic fields. Bremsstrahlung emission in a magnetic field is polarized because the magnetic field breaks the degeneracy in properties of the two natural wave modes, so that information on the field is contained only in the polarized signal. However, in gyroresonant emission the effect is much more direct: it is the acceleration of electrons by the $\mathbf{v} \times \mathbf{B}$ magnetic force itself which produces the

opacity, so that each polarization by itself independently contains information on the magnetic field. Thus bremsstrahlung and gyroresonance emission provide quite different diagnostics. The fact that bremsstrahlung is not a resonant mechanism, the dependence of the polarization of optically–thick bremsstrahlung on the local coronal temperature gradient, and the fact that the polarization of optically–thin bremsstrahlung results from an integration of all contributions along the line of sight, result in the interpretation of bremsstrahlung polarization being less straightforward, but it still provides important complementary information which can be exploited in the study of active regions. At frequencies below 3 GHz bremsstrahlung tends to dominate active region emission and thereby restricts the minimum coronal field strengths which can be studied with gyroresonance emission to about 200 G. We will not discuss bremsstrahlung further here.

In the next section we discuss the basic properties of thermal gyroresonance emission (also known as cyclotron emission), and in the following section we show how these properties determine the radio appearance of solar active regions. We also discuss some of the limitations of radio observations. Many people have contributed over the years to our understanding of gyroresonance emission from the corona, and we will not attempt to ascribe credit for each specific development. Previous papers covering similar topics include Zlotnik (1968a,b), Zheleznyakov (1970), Lantos (1972), Gelfreikh & Lubyshev (1979), Alissandrakis, Kundu & Lantos (1980), Krüger, Hildenbrandt & Fürstenberg (1985), Hurford (1986), Brosius & Holman (1989), Lee, Hurford & Gary (1993), and Vourlidas (1996).

2. The Properties of Gyroresonance Emission

2.1. Physical Mechanism

A collisionless plasma such as the solar corona (where a typical collision frequency, e.g., for a density of $n_e = 10^{10}$ cm^{-3} and temperature $T = 2 \times 10^6$ K, is 200 Hz) may be characterized by two frequencies corresponding to electron resonances: the frequency of oscillation of electrons in the electric field of the ions, known as the plasma frequency, $f_p = 8980\sqrt{n_e}$ Hz; and the gyro frequency, which is the frequency of rotation of an electron about the magnetic field due to the $\mathbf{v} \times \mathbf{B}$ force, $f_B = 2.80 \times 10^6\ B$ Hz, where B is measured in G. For typical conditions in gyroresonant sources above active regions ($n_e = 10^{10}$ cm^{-3} and $B \gtrsim 300$ G), $f_B > f_p$. In such a plasma the propagating electromagnetic modes corresponding to the free–space radiation modes are circularly polarized under most conditions. One of the modes, known as the *extraordinary* or x mode, gyrates about the magnetic field with the same sense of rotation as an electron, and therefore resonates strongly with the thermal electron population; the other mode, known as the *ordinary* or o mode, gyrates about the magnetic field direction with the sense opposite to that of the electron, and correspondingly interacts much less strongly. Since a radiotelescope

can generally detect both modes independently, as opposite circular polarizations, this difference in the strength of interaction of the two modes provides a powerful diagnostic.

The frequency width of a given cyclotron resonance is proportional to $\mu^{-1/2}\, s\, f_B$, where $\mu = m_e c^2/k_B T$. Since $\mu \approx 3000$ in the corona, the cyclotron resonances are very narrow and, for a given value of f_B, opacity is only significant at frequencies very close to discrete harmonics sf_B, s = 1,2,3,... (at much higher temperatures the individual resonances have significant width and may overlap). Equivalently, if we are observing an inhomogeneous corona at a frequency f, gyroresonance opacity is only significant at those discrete points along the line of sight at which $f_B = f/s$, s = 1,2,3,... The thermal width of the cyclotron resonance at coronal temperatures is such that B varies by less than 2% across a resonant layer, corresponding to a physical width of less than 200 km for typical coronal magnetic gradients (scale length $\sim 10^4$ km). The narrow physical thickness of the gyroresonant layers is an important feature of this mechanism: since they are much smaller than relevant gradients in n_e, B and T (except possibly in the vicinity of current sheets), these physical properties may be regarded as constant across any given gyroresonant layer.

2.2. Opacity

The formal expression for gyroresonance opacity is discussed in many places [Zheleznyakov 1970; Melrose 1980; Robinson & Melrose 1984] and will not be derived here. Instead we will simply quote the expression for the optical depth τ of a gyroresonance layer (the absorption coefficient integrated through the layer) as a function of the frequency f, the harmonic number s (which determines $f_B = f/s$ and hence B in the layer), and the angle θ between the magnetic field direction and the line of sight:

$$\tau_{x,o}(s, f, \theta) \;=\; .0133\, \frac{n_e\, L_B(\theta)}{f}\, \frac{s^2}{s!} \left(\frac{s^2\, \sin^2\theta}{2\,\mu} \right)^{s-1} F_{x,o}(\theta) \qquad (1)$$

where $L_B(\theta)$ is the scale length of the magnetic field $(B/\frac{\partial B}{\partial l})$ evaluated along the line of sight. For simplicity we have set the refractive index to be unity in (1). $F_{x,o}(\theta)$ is a function of angle which is of order unity for the x mode near $\theta = 90°$, but decreases sharply at smaller θ, and is smaller in the o mode than in the x mode. At angles θ away from 90° it is often approximated by

$$F_{x,o}(\theta) \;\approx\; (1 \,-\, \sigma\, \cos\theta)^2 \qquad (2)$$

with $\sigma = -1$ for the x mode and $\sigma = 1$ for the o mode. However, this approximation is really only appropriate when the two natural electromagnetic modes are perfectly circularly polarized, and at the low harmonics (s = 1,2,3,4) relevant to the corona this is rarely a good assumption. Zlotnik (1968a) presents accurate expressions for $F_{x,o}(\theta)$ which correctly handle the mode polarization properties. (Note that Zlotnik's formulae are presented in the limit that the refractive index is unity, which introduces a small correction when $f_p \sim f_B$.)

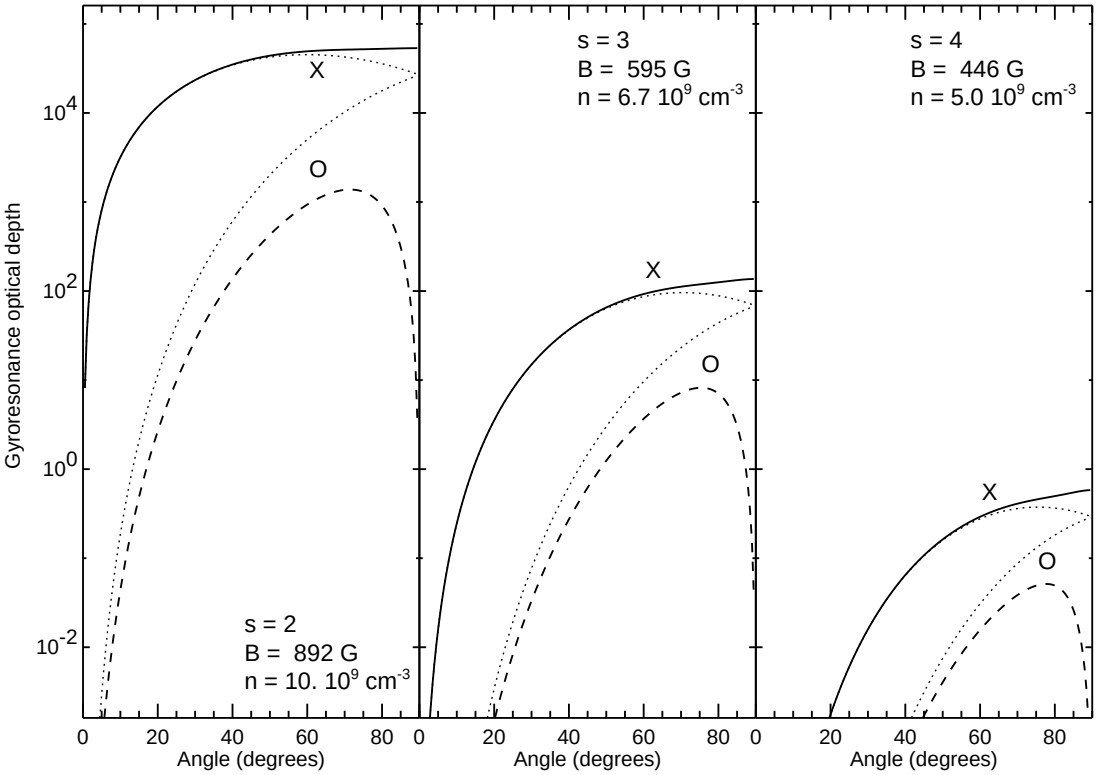

Figure 1. The (integrated) optical depth of the $s = 2$, 3, 4 gyroresonance layers at 5 GHz (left, middle and right panels, respectively) as a function of the angle θ between the line of sight and the magnetic field direction. The temperature in the source is 3×10^6 K, and the magnetic scale height L_B is 10^9 cm. In each panel the solid line is the optical depth of the layer in the x mode, and the dashed line is the optical depth in the o mode. The dotted lines show the optical depth obtained using the circularly–polarized mode approximation (2). The density used for this calculation was decreased as s increases to simulate the decrease of n_e with height: the values are shown in each panel.

In Figure 1 we present exact calculations of τ, the optical depth of a gyroresonant layer, for typical coronal conditions ($T = 3 \times 10^6$ K, $L_B = 10^9$ cm) and a fixed frequency of 5 GHz at the appropriate harmonics $s = 2$, 3 and 4. Both the x (solid lines) and o (dashed lines) modes are shown. For comparison, we also plot the approximation represented by (2) (dotted lines).

A number of features should be noted in this figure:

• For typical coronal conditions, the x mode is optically thick ($\tau \geq 1$) in the $s = 2$ and 3 layers over a broad range of angles θ. The o mode is optically thick over most of the $s = 2$ layer, and may be at least marginally optically thick over a small portion of the $s = 3$ layer if θ is large. Harmonics greater than $s = 4$ do not have any significant optical depth in the quiet solar corona.

• At each harmonic and angle the o mode opacity is always at least an order of magnitude smaller than the x mode opacity, despite the fact that (2) predicts that they should be nearly equal for a range of θ around 90°. The approximation (2) is adequate for the x mode at small θ, but is poor for the o mode at all θ, being easily a factor of 2 or more in error even at small angles.
• The opacity drops sharply towards small θ in both modes. At angles very close to 90°, the o mode opacity dips sharply since it must be a factor of μ smaller than the x mode opacity exactly at $\theta = 90°$ (e.g., Bornatici *et al.* 1983, Robinson 1991). By (1), the opacity is zero at $\theta = 0°$ for $s > 1$. The $\sin^{2s-2}\theta$–dependence of (1) causes the fall–off towards small θ to be much more rapid as s increases.
• For each increase of s by 1, the opacity in a given mode at a given angle drops by slightly more than 2 orders of magnitude. This is largely due to the μ^{-s} dependence of (1). The importance of this large change in opacity from one layer to the next is that a given harmonic layer is likely to be either optically thick over a wide range of angles θ, or else optically thin everywhere.

An important point to be emphasized is that gyroresonance observations are sensitive to the absolute magnetic field strength B, whereas conventional (Babcock or Leighton style) optical magnetographs measure only the line–of–sight component of the magnetic field, $B\cos\theta$, and thus are of limited value for regions near the solar limb. Further, in many cases magnetographs measure magnetic flux averaged over a resolution element (a pixel or a seeing cell) and are thus affected by the filling factor of the magnetic field within the resolution element; radio observations are not affected by this filling factor.

3. Gyroresonance radio emission from active regions

3.1. Radio emission from a dipole magnetic field

Here we will use a dipole magnetic field (vertically–oriented and seen looking directly onto one pole, often used as a model for isolated sunspots) to illustrate the ways in which the properties of gyroresonance emission affect the appearance of solar active regions at microwave frequencies. Figure 2 shows the expected appearance of a a perfectly dipolar field (of peak surface field strength 2500 G) at a frequency of 5 GHz. The upper panel shows the four lowest gyroresonant layers (s = 1, 2, 3, 4, corresponding to B = 1785, 892, 595 and 446 G, respectively), with the line–type indicating whether the layer is optically thick in a given mode. A solid line in the upper panel indicates that the layer is optically thick at both x and o modes; a dashed line indicates that only the x mode is optically thick; and a thin dotted line represents a region of the layer optically thin in both modes. The thin solid lines are magnetic field lines. In the bottom panel we plot the brightness temperature seen by an observer looking straight down on the dipole. In this panel the solid line represents the x mode brightness temperature, which the observer will see as one

circular polarization (right circular polarization if the spot is of positive magnetic polarity), while the dashed line represents the o mode (seen by the observer as the opposite circular polarization).

A height of zero in the atmospheric model used for this calculation corresponds to the base of the corona. The density is 10^{10} cm^{-3} at the base and decreases exponentially with a scale height of 5000 km. The temperature is 6000 K below the corona and 1.0×10^6 K at the base, increasing to 3.0×10^6 K at a height of about 15000 km. The morphology of the radio emission can easily be understood by referring to the gyroresonance (GR) layers and the details of the temperature model, and recalling that along any given line of sight we only see down to the highest optically thick layer:

- Neither mode is optically thick in the $s = 4$ layer, but at the outer edges of this layer there is enough opacity in the x mode to produce a brightness temperature of order 10^5 K, which provides the outer boundary of the radio source.
- On the $s = 3$ layer, the o mode is only (marginally) optically thick at the low–lying outer edge of the layer where θ is largest, but the temperature is relatively low there because of the low altitude. The x mode is optically thick in the $s = 3$ layer to within ~ 5000 km from the center of the umbra, and the peak brightness temperature in the x mode occurs close to the inner edge of this optically–thick region since the height of the layer, and therefore the temperature, is maximum there.
- At smaller radii where the $s = 3$ layer is optically thin, the main contribution to the x mode comes from the $s = 2$ layer which is lower and therefore at a lower temperature: this shows up as a drop in brightness temperature at small radii.
- In the very center of the $s = 2$ layer where the line–of–sight is along the field line, the x mode is optically thin and there is a narrow low–temperature feature. However, it is only a fraction of an arcsecond across and would be difficult to observe.
- In the o mode the central depression in brightness temperature due to the transparency of the $s = 2$ layer at small θ is much broader, and at the center of the spot even the $s = 1$ layer is optically thin in the o mode, but still has sufficient opacity to maintain the brightness temperature at 3.0×10^5 K.
- The sharp features in the o mode profile at radii of order 10^4 km are due to the gap between the radius at which the optically thick $s = 2$ layer drops beneath the corona and the radius at which θ increases sufficiently for the $s = 3$ layer to become (in this case only marginally) optically thick.

3.2. The Effect of Viewing Angle

Since the angle θ is so important in determining the opacity of a GR layer, changing the viewing angle can have a dramatic effect on the appearance of the radio source and this is shown in Figure 3, where we view the same dipolar coronal field at an angle 20° to the vertical. The format of the figure is identical to that of Fig. 2 except that the dipole and the surface have been tilted to show them as the observer would

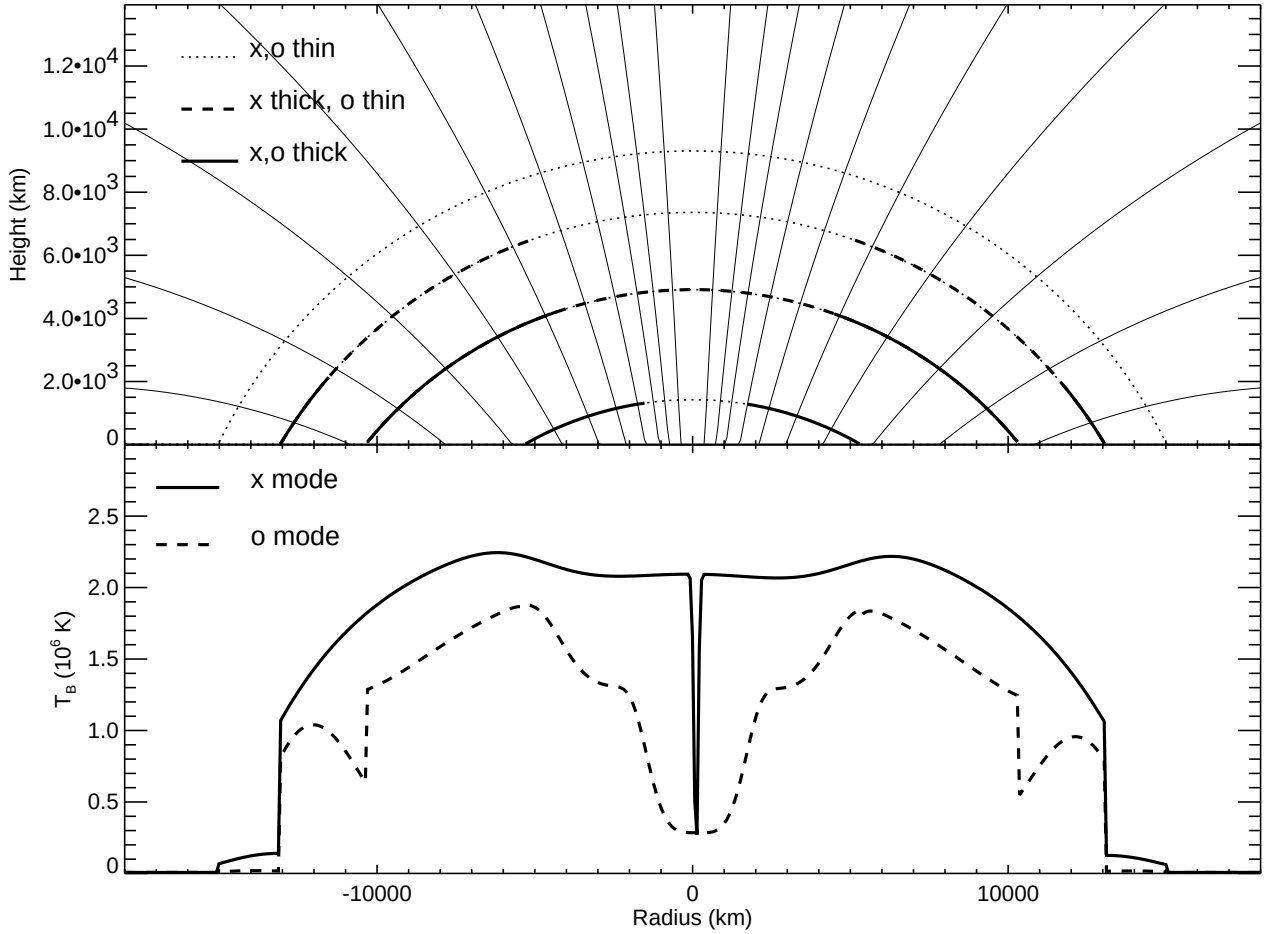

Figure 2. Plots of the gyroresonance layers of a dipole sunspot model (upper panel) and the predicted brightness temperatures resulting from an observation of such a spot (lower panel), viewed nearly vertically (actually 1° off vertical). In the upper panel the thin solid lines are magnetic lines of force and the dotted lines are the $s = 1$, 2, 3, 4 gyroresonance layers, with $s = 4$ the highest and $s = 1$ the lowest layer. Where the gyroresonance layers are optically thick (i.e., $\tau \geq 1$) in the o mode, they have been overplotted with a thick solid line. Except in the $s = 1$ layer where the x mode does not propagate, a layer which is optically–thick in the o mode is also thick in the x mode. If a gyroresonance layer is optically thick in the x mode but not in the o mode, it is overplotted with a thick dashed line. In the lower panel, the x–mode brightness temperature is shown by a solid line and the o mode brightness temperature by a dashed line. The frequency is 5.0 GHz, the dipole is buried at a depth of 1.2×10^9 cm, and the maximum field strength at the surface is 2500 G. In the model temperature increases with radial height from 1.0×10^6 K at the base of the corona (zero height in this case) to 3.0×10^6 K at about 15000 km.

see them. On the far side of the spot from the observer (the left side of this figure) the field lines at the outer edge of the GR layers are nearly orthogonal to the line of sight and this leads to a large opacity in both modes in the $s = 3$ layer there and

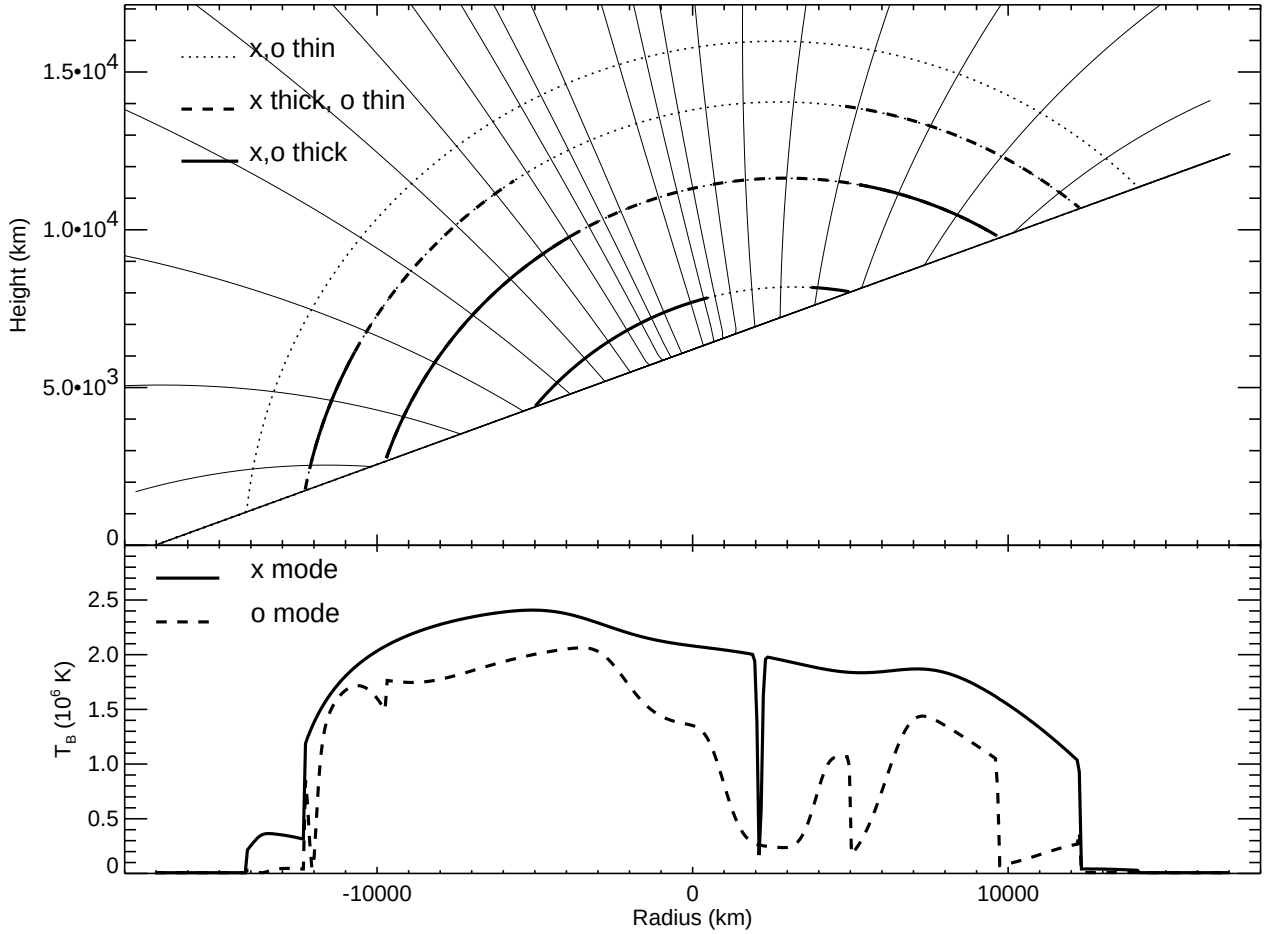

Figure 3. A plot in format identical to Figure 2, except that now the sunspot is viewed from an angle at 20° to the axis of the dipole (the observer is again at the top of the page). The brightness temperature profiles in the bottom panel are shown as the observer would see them in projection.

consequently a relatively small difference in brightness temperature between the two modes. Because the $s = 3$ layer is optically thick to a greater height on the far side where θ is larger, peak brightness temperatures are higher there than on the near side, where the o mode in particular shows structure due to changes in opacity and differences in temperature between the different layers.

3.3. Variation with Frequency

The change in appearance of the radio emission as frequency changes may be seen in Figure 4, where we plot the radio profiles across the dipolar field viewed from directly above in the x (upper panel) and o (lower panel) modes at frequencies from 4 GHz

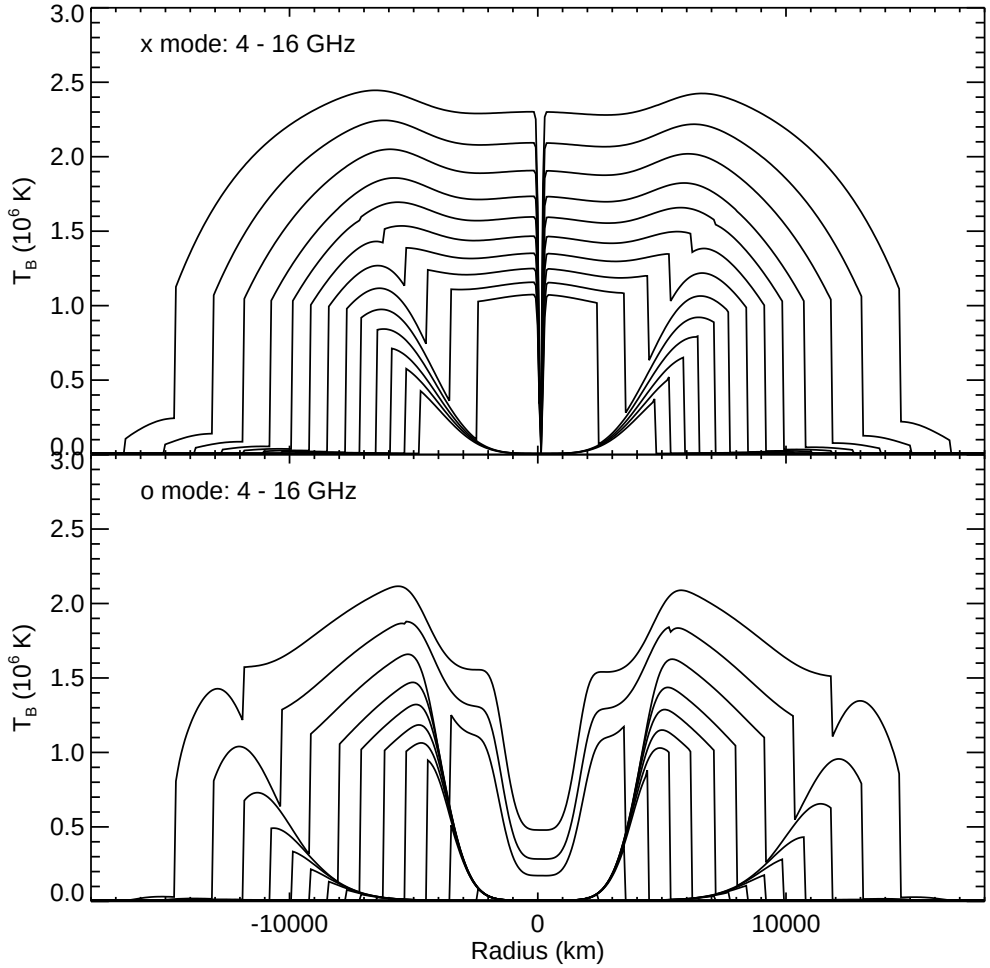

Figure 4. Brightness–temperature profiles across the dipole sunspot model of Figure 2 at frequencies spaced by 1 GHz from 4 to 16 GHz. The upper panel shows the x mode profiles and the lower panel the o mode. In each panel the lowest–frequency profiles are the outside profiles.

(outermost curve) to 16 GHz (innermost curve) at an interval of 1 GHz. Since higher frequencies correspond to stronger magnetic fields, source size decreases as frequency rises. In the o mode the sharp edges at the outer boundaries of the $s = 3$ and $s = 2$ layers are readily evident, changing in dimension as frequency and correspondingly the appropriate value of magnetic field strength change. In the x mode the outer edges of the $s = 3$ and $s = 4$ layers are evident at lower frequencies, while the outer edge of the $s = 2$ layer becomes apparent at higher frequencies. There is a dramatic drop in the peak brightness temperature of the x mode near the center of the spot when the $s = 2$ layer drops below the corona, since the $s = 3$ layer is optically thin at these small viewing angles. The general drop in brightness temperature as

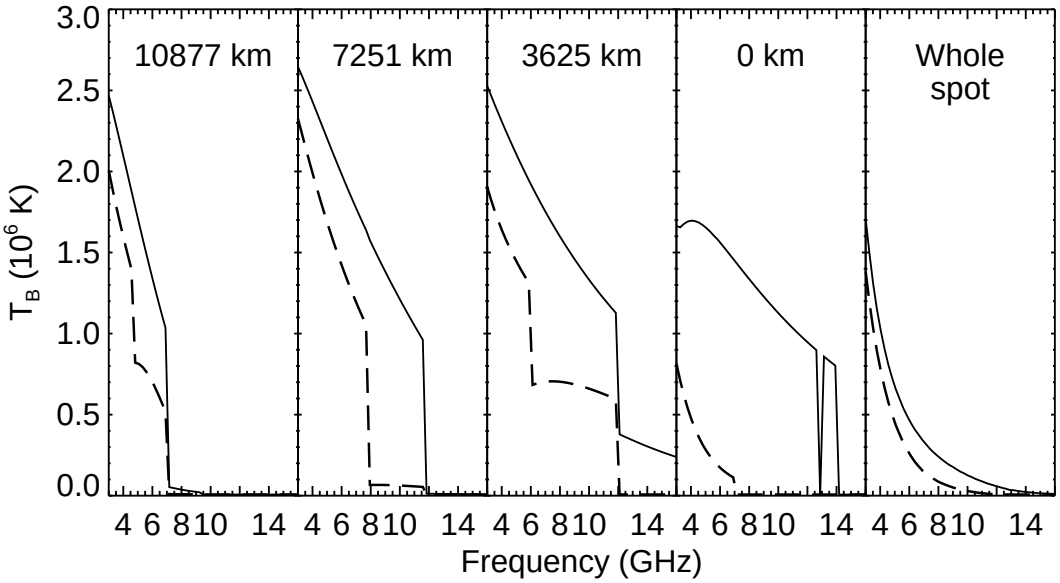

Figure 5. Spectra of the brightness temperature at 4 different locations across the spot in Figure 4 (first 4 panels) and a spectrum averaged across the whole spot (last panel). The spectra are labelled according to their distance from the center of the spot. The x mode brightness temperature is plotted with a solid line and the o mode brightness temperature with a dashed line.

frequency rises is due to the fact that at higher frequencies the GR layers are lower in the corona and therefore, in this model, lie in regions of lower temperature.

Spectra at four different radii and the area-weighted spectrum of the whole spot are shown in Figure 5. Each individual local x mode spectrum is fairly smooth at low frequencies where we simply see the third–harmonic GR layer move down the temperature gradient as f and therefore B increases. The local o mode spectra show more structure due to the different harmonic resonance layers along each line of sight, while the averaged spectrum shows essentially no structure. In all cases for this model the x mode is brighter than the o mode since, on average, the x mode opacity occurs higher up the temperature gradient.

The influence of the temperature structure in the corona on the appearance of microwave images may be seen in Figure 6. Whereas in Fig. 4 the temperature increased monotonically with height, the temperature in the model used in Fig. 6 is 1.0×10^6 K at the base but then peaks at 3.0×10^6 K at a height of 4000 km, and declines with further increase in height to an asymptotic value of 1.0×10^6 K. By contrast with Fig. 4, where lower frequencies invariably produced higher brightness temperatures because they arose higher in the corona and therefore higher on the temperature gradient, in Fig. 6 we see curves for different frequencies in the same mode cross one another as different portions of a gyroresonant layer pass through the temperature peak at a height of 4000 km. Also, whereas the radio source was everywhere x–mode polarized in Fig. 4, in Fig. 6 there are regions where the o mode

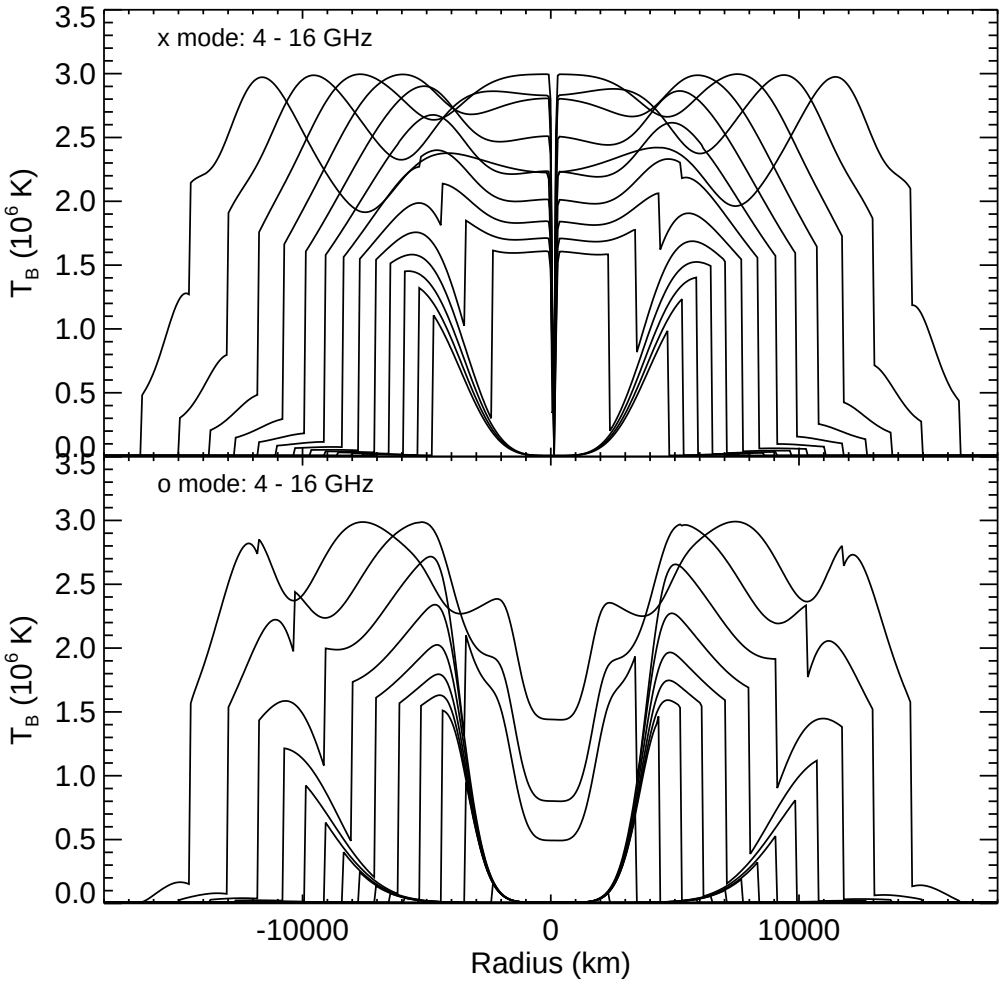

Figure 6. Brightness–temperature profiles across a model sunspot with the dipolar magnetic field configuration of Figure 2 but with a different coronal temperature gradient: in this case the temperature rises from about 2.0×10^6 K at the base of the corona to 3.0×10^6 K at 4000 km, and then decreases to 1.0×10^6 K at about 8000 km. As in Fig. 4, curves are plotted at frequencies spaced by 1 GHz from 4 (outermost curve) to 16 GHz (innermost curve). The upper panel shows the x mode profiles and the lower panel the o mode.

is brighter than the x mode because the o mode is optically thick in the $s = 2$ layer close to the temperature maximum while along the same line of sight the x mode is optically thick in the higher $s = 3$ layer, well above the coronal temperature maximum. Vourlidas (1996) interprets a detection of o mode polarization from a sunspot in terms of a temperature structure of this type. At high frequencies, where all the important GR layers lie below a height of 4000 km, the pattern reverts to one very similar to Fig. 4.

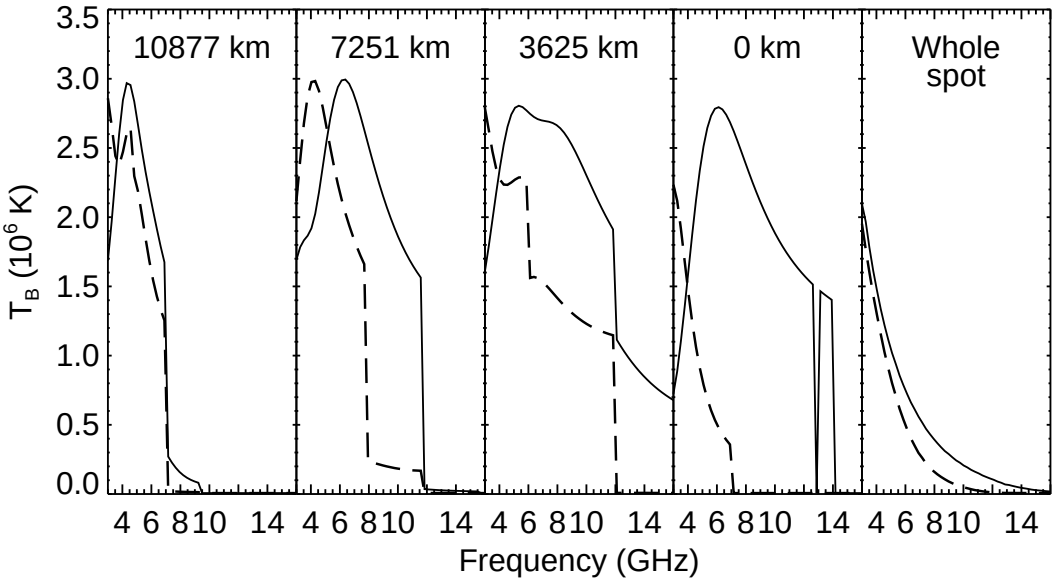

Figure 7. Spectra of the brightness temperature at 4 different locations across the spot in Figure 6 (first 4 panels) and a spectrum averaged across the whole spot (last panel). The spectra are labelled according to their distance from the center of the spot. The x mode brightness temperature is plotted with a solid line and the o mode brightness temperature with a dashed line.

The potential for polarization signatures to reveal the temperature structure is further emphasized in Figure 7, where we plot spectra corresponding to different locations in Fig. 6 (the format is identical to that of Fig. 5). Here we see that at any location the x mode dominates at high frequencies, where there is no significant o mode opacity; but at low frequencies where opacity is large in both modes, the o mode is in most cases brighter than the x mode at the lowest frequencies. This is true everywhere except at very large radii where the x mode has significant opacity in the fourth harmonic layer while the o mode does not (Fig. 6). For this reason the area–weighted spectrum still remains slightly x mode polarized at low frequencies.

The structure revealed at many closely–spaced frequencies in these models shows that appropriate observations contain a great deal of information about both the magnetic field and temperature of the corona. The contrast between the local spectra and the mean spectrum of the spot indicates the value of high spatial resolution in studies of this kind.

3.4. Observational examples

We have used a dipolar magnetic field with simple temperature gradients as examples here because they are particularly straightforward to calculate, but the basic principles apply to all gyroresonance emission. Rarely do actual observations show the straightforward structure of our models. Isolated sunspots viewed near the cen-

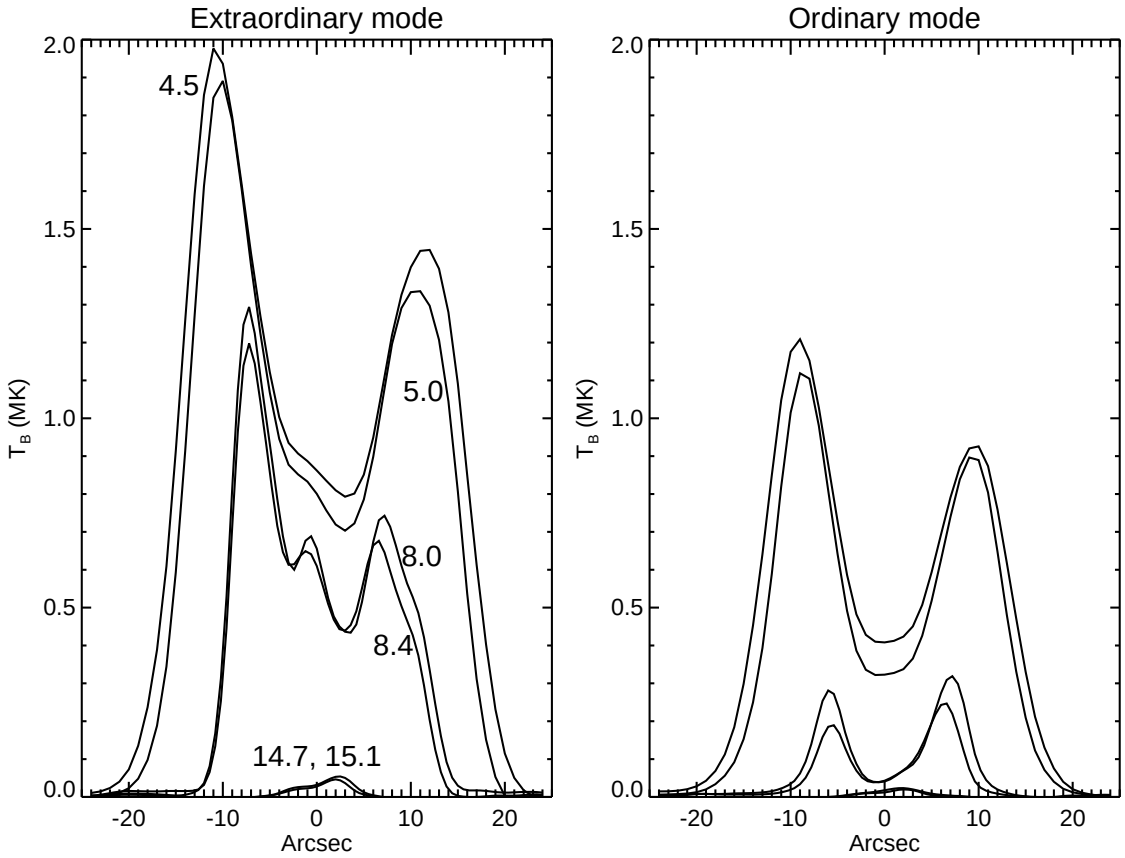

Figure 8. Brightness–temperature profiles across an isolated sunspot observed near disk center (actually 13° north–west of disk center) with the VLA by Zlotnik et al. (1996). The 6 curves each show the brightness temperature along a cut across the source at a different frequency, starting with 4.5 GHz as the outermost curve, and 14.7 & 15.0 GHz as the two innermost curves. The curves are labelled according to frequency in the left panel which shows the x mode; the right panel shows the corresponding o mode profiles, which are present in the same order as in the left panel.

ter of the disk can show the basic pattern of a symmetric ring of emission, with low brightness temperatures over the umbra where θ is small. An example of profiles from such a sunspot is shown in Figure 8, taken from Zlotnik *et al.* (1996). This is a VLA[1] observation with data at the frequencies 4.5, 5.0, 8.0, 8.4, 14.7 and 15.0 GHz. At the two highest frequencies there are no optically–thick GR layers in the corona and brightness temperatures remain low. In general we see that the brightness temperature decreases steadily as frequency increases, and the x mode brightness temperature everywhere exceeds the o mode brightness temperature at the same frequency. As discussed in the previous section, this combination of properties suggests

[1] The VLA is a facility of the National Radio Astronomy Observatory, which is operated by Associated Universities, Inc., under cooperative agreement with the National Science Foundation.

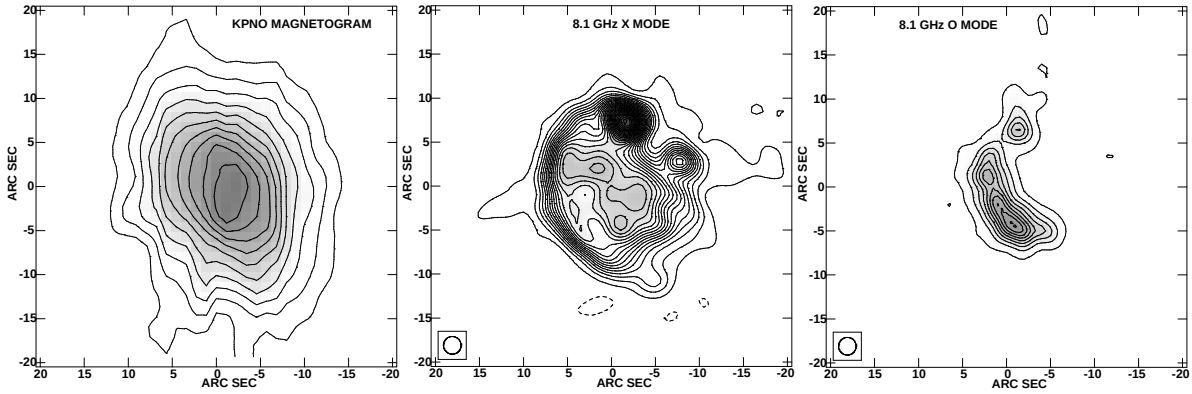

Figure 9. Images of a simple sunspot obtained on 1993 August 17. The left panel shows the line–of–sight photospheric magnetic field from a magnetogram obtained at the Kitt Peak National Observatory; contours are at 100 G intervals with a lowest contour of 100 G. The strongest longitudinal magnetic field measured in the spot is of order 1080 G. Radio images obtained with the VLA at 8.1 GHz are shown in the middle (x mode) and right (o mode) panels. In both radio images the bottom contour is at 25×10^4 K and successive contours are 50×10^4 K apart. The peak brightness temperature in the x mode image is 1.42×10^6 K and the peak brightness temperature in the o mode is 0.43×10^6 K. Disk center is towards the upper right quadrant, $300''$ north and $270''$ west of the spot at the time. The beam size in the radio images is $2''.0$.

a positive gradient of temperature with height, at least over the range of heights covered by these observations. The central depression in the x mode is far broader than the corresponding feature in Fig. 4. This can be explained if the temperature has a radial dependence, i.e., the corona over the umbra is cooler than over the penumbra (in Fig. 4 the temperature has no radial dependence). Another feature which is not consistent with the simple models is that the radio emission is brighter on the eastern side, closer to disk center, whereas in an atmosphere with a positive temperature gradient viewed at a moderate angle (e.g., Fig. 3), we expect the side away from disk center to have brighter radio emission. In these observations, the spatial resolution, although excellent (several arcseconds), is probably inadequate to see the sharp edges at resonance layer jumps seen in Figure 4.

As a second example, Figure 9 shows VLA x and o mode images of a simple sunspot at a single frequency, 8.1 GHz, together with a photospheric magnetogram taken by Kitt Peak National Observatory. The sunspot was located at heliocentric coordinates S17E18 (heliographic coordinates S10E18) at the mid–time of the radio observation, so apparent disk center is towards the top right corner of the images. If the sunspot fields are radial at the center of the spot and diverge away from the center, then we are viewing the magnetic field largely at small θ (i.e., low opacity) on the north-west side of the spot, and preferentially at large θ (large opacity) on the south–east side. This probably explains the asymmetry seen in the x mode source, which is clearly brighter to the south–east than the north–west. As in Fig. 8, the x mode is everywhere brighter than the o mode, and the x mode source is

much larger than the o mode source. There are sharp edges to the x mode source, particularly on the south–eastern side where we expect it to be optically thick out to the boundary of the GR layer; on the north–western side the more gradual fall–off in brightness temperature may be due to the variation of θ. Note that there are small discrete features around the penumbra, including the brightest feature in the x mode image at the northern tip of the penumbra, which clearly do not fit a simple dipole pattern. A soft X–ray image shows a bright loop emerging from the spot penumbra at the location of the brightest feature, so this may well be a region where the enhanced density and temperature associated with the loop overcome the effect of small θ and elevate the optical depth where it would otherwise be low. Within the main body of the x mode source is a central broad and relatively flat ridge of emission which is $\sim 2 \times 10^5$ K brighter than a small trough to the east (6×10^5 K), beyond which is the bright eastern rim of the sunspot radio source. It is possible that these features represent different GR layers. The main ridge of the o mode source essentially coincides with the brightest fields measured in the magnetogram. The peak line–of–sight field in the magnetogram is only 1070 G, so it is not plausible that the o mode emission arises at the fundamental GR layer (2880 G) and it is more likely to be second harmonic emission (1440 G), while much of the x mode source is probably third harmonic emission (960 G).

Both the examples used here are of simple sunspots since they most closely resemble our model calculation and therefore most straightforwardly illustrate the concepts discussed earlier. Most active regions of interest are far more complicated, and the previous published radio images of active regions (too numerous to refer to here: see White *et al.* 1992 for a list of studies published prior to 1992) show the full range of complexity. However, we emphasize that there is no difference in principle between the simple dipole model and a real active region: in the latter, as in the former, it is the interplay between the the structure of the GR layers (particularly the variation of θ over the layers) and the temperature and density structure of the corona which determines the appearance of an active region at microwave frequencies. Much of the diagnostic potential of gyroresonance emission lies in the fact that at a given frequency it reveals specific well–defined layers, and this is equally true of simple dipolar sunspots and real active regions with more convoluted GR layers.

4. Applications of Gyroresonance Emission

4.1. Coronal magnetic field measurement

One of the simplest uses of radio observations is the determination of magnetic field strengths at the base of the corona (e.g., Hurford 1986). The absolute value of the coronal magnetic field strength is important for understanding the energetics of the corona, and the availability of free energy stored in coronal magnetic fields which may be used in flares and coronal heating. Figs. 2-7 demonstrate that where the optically–thick GR layer corresponding to a given frequency and mode drops below the corona,

the radio brightness temperature at that frequency and corresponding polarization shows a sharp drop from coronal to approximately chromospheric values. (Note that the transition region is not expected to be detected via gyroresonance emission if its thickness is less than $1''$ as energy balance models predict, because its signature would be confined to the line at the intersection of the $< 1''$–thick surface of the transition region with the typically $< 0''.2$–thick GR surface, and the thickness of this line is likely to be so narrow as to be undetectable.) Observationally it is a simple matter to detect such a signature. Thus the locations of the outer edges of the radio sources at differing frequencies contain information on the magnetic field strength at the base of the corona. With data such as those shown in Figs. 4–7, several harmonics can be identified unambiguously in each mode and therefore the appropriate values of s can be identified, which is essential to determine absolute values of B. In this way, it is straightforward to map the distribution of B over the base of the corona wherever the radio emission is dominated by bright gyroresonance emission. This technique has been convincingly demonstrated with the Owens Valley frequency–agile interferometer [Gary & Hurford 1994].

When only a few frequencies are available, as in VLA observations, it is possible to map the extent of the region in the corona in which the magnetic field exceeds the values which correspond to the frequencies observed. High–frequency observations allow us to estimate the maximum magnetic field strength in the corona. This can be obtained from the maximum frequency f_m GHz at which coronal brightness temperatures are observed, using the assumption that this will take place in the x mode in the $s = 3$ layer at the base of the corona where the field strength is maximum. (One feature illustrated by Figure 1 is that only in extreme conditions is the $s = 4$ layer optically thick, and therefore $s = 3$ is generally appropriate for this purpose.) On this assumption, the maximum field strength is $120\, f_m$ G. For example, if as in White et al. (1991) there are coronal brightness temperatures at 15 GHz, the coronal magnetic field must reach at least 1800 G. When the 17 GHz Nobeyama radioheliograph measures coronal brightness temperatures from an active region, the coronal magnetic field must exceed 2000 G [Shibasaki *et al.* 1994]. When many closely-spaced frequencies have been observed, as is possible with the Owens Valley frequency–agile interferometer and RATAN–600, fairly tight limits can be placed on the maximum magnetic field strength [Akhmedov *et al.* 1982; Lee *et al.* 1993; Gary & Hurford 1994].

4.2. Coronal currents

An extension of this simple measurement is the identification of coronal currents. Coronal currents generate magnetic fields and therefore elevate coronal field strengths above the values expected from simple potential–field (i.e., current–free) extrapolations of surface measurements. They will also produce a characteristic reversal of field direction with position as one moves across the current layer. Both these features are in principle observable in radio images. Relatively little has been done in this area

due to the difficulties of obtaining well–calibrated, unsaturated photospheric magnetogram data simultaneous with suitable radio data (i.e., at high spatial resolution and covering the appropriate frequency range), and the problem of identifying the height of the radio source [Alissandrakis *et al.* 1980; Schmahl *et al.* 1982; Alissandrakis & Kundu 1984; Chiuderi Drago *et al.* 1987; Schmelz *et al.* 1994]. Recently Lee *et al.* (1996) have shown a compelling example in which potential extrapolations of photospheric magnetic fields were unable to explain the presence of a 15 GHz radio source over a neutral line even with the conservative assumption that the 4th harmonic layer could have sufficient opacity to be optically thick (requiring 1330 G fields). In this case a photospheric vector magnetogram also indicates the presence of a strong current with footpoints in the photosphere on either side of the neutral line and consistent with a coronal current crossing the neutral line in the corona at the location inferred from the radio data. In this case the radio data also happen to be useful for resolving the 180° ambiguity in the photospheric magnetogram data [Lee *et al.* 1996].

Since coronal currents are implicated in both coronal heating and solar flares, this application of radio observations is potentially very valuable, and we expect this to be an area of focus in coming years.

4.3. Heights of radio sources

Perhaps the major shortcoming of gyroresonance emission as a diagnostic is the fact that it does not yield height information directly. (Other coronal diagnostics such as X–ray imaging share this shortcoming.) A single radio observation at multiple frequencies is sensitive to emission from many different GR layers in the corona, but is largely insensitive to the distance between the layers, and for this reason does not easily lend itself to height determination. When two observations at different times are combined, the change in perspective produced by solar rotation permits stereoscopy to be used to estimate source heights [Aschwanden & Bastian 1994]. However, to carry this out correctly for gyroresonance emission requires both that the physical properties of the corona not change between the observations and that the changes in appearance expected from the dependence on θ be taken into account carefully, which is far from trivial.

In principle there is information present on the heights of the GR layers due to the dependence of the optical depth (1) on L_B, and the fact that we know the magnetic field strength in each layer. L_B must be consistent with the height separation of isogauss layers of different field strengths. If L_B could be determined from the data, it may be possible to use the combination of L_B, the fundamental law $\nabla \cdot \mathbf{B} = 0$ and the fact that B is constant within a layer to reconstruct the heights of the GR layers, at least approximately. However, in (1) L_B is coupled with the electron density, and it may be difficult to separate these two parameters from radio data alone: EUV observations which provide independent information on n_e, and

improved extrapolations of surface fields which provide an estimate of L_B, may help with this separation.

4.4. Comparison with other methods

No other method can measure coronal magnetic field strengths. There is considerable progress in our understanding of the extrapolation of photospheric field measurements into the corona, including the effects of currents, but no technique yet exists which claims to do this perfectly. Further, the most common techniques for measuring photospheric fields are susceptible to errors which will contaminate the extrapolations.

Despite suffering from the problem of all optically–thin diagnostics, line–of–sight confusion, soft X–ray imaging observations can be extremely valuable for studies of coronal magnetic fields because, when density contrast between neighbouring field lines is sufficient, they show the (projected) paths of field lines in the corona. This can be particularly useful for resolving the well–known 180deg ambiguity in vector magnetic field observations. Radio observations are less likely to show field lines directly because gyroresonance emission tends to be optically thick and therefore is more sensitive to temperature contrast rather than density contrast.

However, soft X–ray data are much less sensitive to absolute values of magnetic field strength. In their comparison of radio images with extrapolations of photospheric magnetic field observations, Lee *et al.* (1996) discuss the effects of errors in the magnetogram on the resulting magnetic field images. Two of the most common problems in Babcock–style magnetographs are stray light contamination and saturation in the dark regions of sunspot umbrae. Stray light has the effect of diminishing inferred magnetic field strengths by roughly the same factor everywhere, while saturation leads to underestimation of the strongest field strengths in sunspots. Corrections for these effects raise field strength values in the active region considerably, but potential extrapolations show that they do not change the topology of the field lines significantly. Since soft X–ray observations only show field lines, comparisons between soft X–ray observations and photospheric longitudinal magnetograms are not very sensitive to errors in the magnetograms, whereas radio observations are sensitive to such errors since the increased field strengths change the locations of the GR layers. In particular, the question of whether sufficient field strengths are present in the corona to explain high–frequency radio sources at all will be affected by such errors.

5. Propagation effects

As noted earlier, the polarization of the natural modes in the corona changes with the angle θ between the propagation direction and the magnetic field. At small θ the modes are purely circularly polarized; at $\theta = 90°$ they are purely linearly

polarized. As radiation propagates through the corona θ will change and two things can happen: the radiation can retain its polarization, or it can retain its mode identity and therefore change polarization as θ changes. Away from $\theta = 90°$, the former is generally true, i.e., *strong mode coupling* operates: the radiation can couple easily from one mode to the other and as it propagates it is apportioned between the two (changing) local modes such that its original sense of polarization is preserved. However, where θ passes though 90° (known as the *quasi–transverse* or QT layer), the sense of circular polarization can reverse: effectively, if the transition from the natural modes being circularly polarized to being linearly polarized is gradual, then mode coupling is *weak*, mode identity is retained across the layer, and the radiation emerging from the layer has the opposite sense of circular polarization from that with which it entered (because the sign of $\cos\theta$ has changed). On the other hand, if the transition is abrupt, coupling between the modes will be strong and the sense of polarization will be preserved.

Mode coupling is a strong function of frequency and magnetic field: the coupling coefficient is proportional to $f^4/{f_B}^3 f_p$, so coupling tends to be strong at large heights and weak at low heights. For a bipolar active region near the limb, radiation from the limbward side of the region must pass through a QT region at low altitude on its way to a terrestrial observer, and for typical conditions at microwave frequencies we expect weak coupling and therefore polarization reversal. This is clearly seen in many observations (e.g., Kundu & Alissandrakis 1984). This presents both a complication and an opportunity for studies of active regions. The complication is that it introduces some uncertainty in determining the true sense of polarization of the radio emission in the source from the polarization observed at a terrestrial telescope, particularly at frequencies between 3 and 10 GHz (coupling should usually be strong at high frequencies thanks to the f^4–dependence of the coupling coefficient). However, in practice observers are generally able to recognize the presence of weak mode coupling by comparing the large–scale pattern of radio polarization with optical magnetograms, and ambiguity is rarely a problem. Once the boundary between weak and strong mode coupling has been identified, it can be used as a diagnostic of plasma conditions in the coupling layer, using the known form of the coupling coefficient [Bandiera 1982; Kundu & Alissandrakis 1984; Gelfreikh *et al.* 1987].

We have not discussed linear polarization in this review because it is not generally detected: another important propagation effect acts to wash out any linear polarization which may originally have been present in the radiation (in general gyroresonance emission will contain both circular and linear polarization, depending on the local nature of the natural modes in the source). As mentioned above, for most of the propagation path through the corona the natural modes are circularly polarized, and the information on any linear polarization present is contained in the relative phase between the x and o modes. However, the two modes have slightly different refractive indices which cause the electric fields in the modes to rotate at slightly different rates even though they have the same frequency. In the solar corona the observing frequency is generally not that far from the plasma frequency, and in

that case the difference in refractive index is relatively large and is a strong function of frequency. We observe the Sun using radio receivers of a finite bandwidth, and the difference in rotation rates across the bandwidth received is so large that all coherence is lost and the information on linear polarization is wiped out: the component of the radiation which was linearly polarized in the source becomes unpolarized. This effect is known as *differential Faraday rotation*. In principle one can detect linear polarization by using a sufficiently small bandwidth, and there has been a recent report of such a detection [Alissandrakis & Chiuderi-Drago 1994; Alissandrakis & Chiuderi-Drago 1995].

6. Summary

Gyroresonance emission offers a potentially very powerful tool for the study of coronal magnetic fields. The reason for its power lies in the combination of two factors: (i) it is a resonant mechanism, which means that at any given frequency only a small number of isogauss surfaces, which may be regarded as thin and homogeneous, contributes to the emission. This is in contrast to optically–thick bremsstrahlung, which is not resonant and may have a "skin–depth" (the depth over which it becomes optically thick) which is comparable to the scale length of gradients in T and n_e. The fact that a significant thickness of corona contributes to bremsstrahlung emission leads to formal inversion difficulties similar to those faced in the inversion of hard X–ray spectra, where electrons over a broad range of energies contribute at a single photon energy (e.g., Craig & Brown 1986). The discrete nature of optically thick GR layers avoids similar problems. (ii) Gyroresonance emission is optically thick, which means that along any given line of sight in one polarization we are sampling only the properties in that very narrow harmonic GR layer which happens to dominate along that line of sight: by using many closely spaced frequencies, we can peel away successive layers of the corona, revealing the magnetic, temperature and density structure as a function of height. This combination of properties is not shared by any other means for viewing the corona, and it has clear advantages over optically thin diagnostics, such as X–rays, for many purposes.

At present we are unable to exploit fully the potential of such observations for want of a suitable instrument. The Owens Valley frequency–agile interferometer has convincingly demonstrated the potential of multifrequency observations [Gary & Hurford 1994], while models and VLA observations show that there is structure present in the corona on very fine spatial scales which require a large multi–element interferometer if they are to be imaged successfully. This has in part motivated plans for a new solar–dedicated radio telescope which will combine the imaging quality of the VLA (suitably improved–upon) with the frequency capability of the Owens Valley frequency–agile interferometer [Gary & Bastian 1996], and will be capable of making observations at least as good as those modelled in Figures 4–7.

When such a telescope exists, the challenge confronting us will be to "invert" the multi–frequency radio images in order to extract as much information as possible from them regarding the spatial structure of coronal magnetic fields, temperature distributions and density distributions. No such robust inversion technique exists at present, although in individual studies many researchers have shown that different individual pieces of the puzzle can be solved (such as the distribution of B at the base of the corona, mentioned earlier). Combination of radio data with other wavelengths has the potential for greatly enhancing our ability to exploit the radio data. For example, if photospheric magnetograms were error–free and could reliably be extrapolated to give the coronal magnetic fields, determination of the temperature and density structure of the corona would be greatly simplified. In general this is not yet the case: a more likely scenario is that extrapolations of photospheric magnetic data will be used as a first approximation to the coronal field, and this will be adjusted iteratively as part of the analysis process. Exploring methods for inversion such as this will occupy the modellers in coming years while the observers work towards a new telescope.

Acknowledgements

This review represents (some of) the acquired experience of many people working in this field, too numerous to mention here. We thank Jeongwoo Lee for his encouragement and valuable discussions, and S. T. Wu and Pat Corder for their organization of the SCOSTEP Workshop on *Measurements and Analyses of the 3D Solar Magnetic Fields*. This work is supported by NSF grant ATM 93–16972 and NASA grant NAG–W–1541.

References

Akhmedov, S. B., Gelfreikh, G. B., Bogod, V. M., & Korzhavin, A. N.: 1982, *Solar Phys.* **79**, 41.
Alissandrakis, C., & Chiuderi-Drago, F.: 1994, *Astrophys. J. (Lett.)* **428**, L73.
Alissandrakis, C., & Chiuderi-Drago, F.: 1995, *Solar Phys.* **160**, 171.
Alissandrakis, C. E., & Kundu, M. R.: 1984, *Astron. Astrophys.* **139**, 271.
Alissandrakis, C. E., Kundu, M. R., & Lantos, P.: 1980, *Astron. Astrophys.* **82**, 30.
Aschwanden, M. J., & Bastian, T. S.: 1994, *Astrophys. J.* **426**, 425.
Bandiera, R.: 1982, *Astron. Astrophys.* **112**, 52.
Bornatici, M., Cano, R., De Barbieri, O., & Engelmann, F.: 1983, *Nucl. Fusion* **23**, 1153.
Brosius, J. W., & Holman, G. D.: 1989, *Astrophys. J.* **342**, 1172.
Chiuderi Drago, F., Alissandrakis, C. E., & Hagyard, M.: 1987, *Solar Phys.* **112**, 89.
Craig, I. J. D., & Brown, J. C.: 1986, *Inverse Problems in Astronomy*, Adam Hilger, Bristol.
Gary, D. E., & Bastian, T. S.: 1996, *Report of the Solar Radio Telescope Workshop*, in preparation.
Gary, D. E., & Hurford, G. J.: 1994, *Astrophys. J.* **420**, 903.
Gelfreikh, G. B., & Lubyshev, B. I.: 1979, *Sov. Astron.* **23**, 316.
Gelfreikh, G. B., Peterova, N. G., & Ryabov, B. I.: 1987, *Solar Phys.* **108**, 89.
Ginzburg, V. L., & Zheleznyakov, V. V.: 1961, *Sov. Astron.* **5**, 1.
Hurford, G. J.: 1986, in E. Tandberg-Hanssen, R. M. Wilson, & H. S. Hudson (eds.), *Solar Flares & Coronal Physics Using P/OF as a Research Tool*, NASA Conf. Pub. 2421, p. 191.
Kakinuma, T., & Swarup, G.: 1962, *Astrophys. J.* **136**, 975.
Krüger, A., Hildebrandt, J., & Fürstenberg, F.: 1985, *Astron. Astrophys.* **143**, 72.
Kundu, M. R., & Alissandrakis, C. E.: 1984, *Solar Phys.* **94**, 249.
Lantos, P.: 1972, *Solar Phys.* **22**, 387.
Lee, J., White, S. M., Gopalswamy, N., & Kundu, M. R.: 1996, *Solar Phys.*, submitted.
Lee, J. W., Hurford, G. J., & Gary, D. E.: 1993, *Solar Phys.* **144**, 45.
Melrose, D. B.: 1980, *Plasma Astrophysics*, Gordon and Breach, New York.
Robinson, P. A.: 1991, *Solar Phys.* **136**, 343.
Robinson, P. A., & Melrose, D. B.: 1984, *Aust. J. Phys.* **37**, 675.
Schmahl, E. J., Kundu, M. R., Strong, K. T., Bentley, R. D., Smith, J. B., and Krall, K. R.: 1982, *Solar Phys.* **80**, 233.
Schmelz, J. T., Holman, J. D., Brosius, J. W., & Willson, R. F.: 1994, *ApJ* **434**, 786.
Shibasaki, K., Enome, S., Nakajima, H., Nishio, M., Takano, T., Hanaoka, Y., Torii, C., Sekiguchi, H., , Kawashima, S., Bushimata, T., Shinohara, N., Koshiishi, H., Shiomi, Y., Irimajiri, Y., Leka, K. D., & Canfield, R. C.: 1994, *Publ. Astron. Soc. Japan* **46**, L17.
Vourlidas, A.: 1996, *Ph. D. thesis*, New Mexico Inst. of Mining and Technology, unpublished.
White, S. M., Kundu, M. R., & Gopalswamy, N.: 1991, *Astrophys. J. (Lett.)* **366**, L43.
White, S. M., Kundu, M. R., & Gopalswamy, N.: 1992, *Astrophys. J. Supp.* **78**, 599.
Zheleznyakov, V. V.: 1962, *Sov. Astron. AJ* **6**, 3.
Zheleznyakov, V. V.: 1970, *Radio Emission of the Sun and the Planets*, Pergamon Press Ltd., Oxford.
Zlotnik, E. Y.: 1968a, *Sov. Astron.* **12**, 245.
Zlotnik, E. Y.: 1968b, *Sov. Astron.* **12**, 464.
Zlotnik, E. Y., White, S. M., Kundu, M. R., & Zheleznyakov, V. V.: 1996, *Astrophys. J.*, in preparation.